References and Notes

1. G. S. Salvesen, C. S. Duckett, *Nat. Rev. Mol. Cell Biol.* **3**, 401 (2002).
2. D. Vucic, W. J. Fairbrother, *Clin. Cancer Res.* **13**, 5995 (2007).
3. G. S. Salvesen, J. M. Abrams, *Oncogene* **23**, 2774 (2004).
4. J. N. Dynek, D. Vucic, *Cancer Lett.* (2010).
5. A. M. Hunter, E. C. LaCasse, R. G. Korneluk, *Apoptosis* **12**, 1543 (2007).
6. S. W. Fesik, *Nat. Rev. Cancer* **5**, 876 (2005).
7. C. Du, M. Fang, Y. Li, L. Li, X. Wang, *Cell* **102**, 33 (2000).
8. A. M. Verhagen *et al.*, *Cell* **102**, 43 (2000).
9. J. A. Flygare, W. J. Fairbrother, *Expert Opin. Ther. Pat.* **20**, 251 (2010).
10. Z. Liu *et al.*, *Nature* **408**, 1004 (2000).
11. G. Wu *et al.*, *Nature* **408**, 1008 (2000).
12. A. Gaither *et al.*, *Cancer Res.* **67**, 11493 (2007).
13. E. Varfolomeev *et al.*, *Cell* **131**, 669 (2007).
14. J. E. Vince *et al.*, *Cell* **131**, 682 (2007).
15. C. Ndubaku *et al.*, *ACS Chem. Biol.* **4**, 557 (2009).
16. T. K. Oost *et al.*, *J. Med. Chem.* **47**, 4417 (2004).
17. K. Zobel *et al.*, *ACS Chem. Biol.* **1**, 525 (2006).
18. J. W. Blankenship *et al.*, *Biochem. J.* **417**, 149 (2009).
19. T. Samuel *et al.*, *J. Biol. Chem.* **281**, 1080 (2006).
20. E. Varfolomeev, S. M. Wayson, V. M. Dixit, W. J. Fairbrother, D. Vucic, *J. Biol. Chem.* **281**, 29022 (2006).
21. R. J. Deshaies, C. A. Joazeiro, *Annu. Rev. Biochem.* **78**, 399 (2009).
22. P. D. Mace, S. Shirley, C. L. Day, *Cell Death Differ.* **17**, 46 (2010).
23. P. D. Mace *et al.*, *J. Biol. Chem.* **283**, 31633 (2008).
24. R. Kulathila *et al.*, *Acta Crystallogr. D Biol. Crystallogr.* **65**, 58 (2009).
25. R. Feltham *et al.*, *J. Biol. Chem.* **286**, 17015 (2011).

Acknowledgments: We thank C. Yu, P. Lupardus, Shamrock Structures LLC, and staff at the Advanced Light Source, the Stanford Synchrotron Radiation Lightsource (SSRL) and the Advanced Photon Source at Argonne National Laboratory for their assistance with sample handling and data collection. The Advanced Light Source is supported by the Director, Office of Science, Office of Basic Energy Sciences, of the U.S. Department of Energy (DOE) under contract no. DE-AC02-05CH11231. SSRL is a Directorate of SLAC National Accelerator Laboratory and an Office of Science User Facility operated for the DOE Office of Science by Stanford University. The SSRL Structural Molecular Biology Program is supported by the DOE Office of Biological and Environmental Research and by the Biomedical Technology Program, National Center for Research Resources, NIH (P41RR001209). Use of the Advanced Photon Source, a facility operated for DOE Office of Science by Argonne National Laboratory, was supported under contract no. DE-AC02-06CH11357. We also thank the Microchemistry and Proteomics Laboratory and the Oligo Synthesis and DNA Sequencing facilities at Genentech for their technical support. Atomic coordinates and structure factors have been deposited in the Protein DataBank with accession code 3T6P. Reagents are available from Genentech subject to a material transfer agreement.

Supporting Online Material

www.sciencemag.org/cgi/content/full/334/6054/376/DC1
Materials and Methods
Figs. S1 to S12
Tables S1 and S2
References (*26*–*37*)

3 May 2011; accepted 15 September 2011
10.1126/science.1207862

Mass Spectrometry of Intact V-Type ATPases Reveals Bound Lipids and the Effects of Nucleotide Binding

Min Zhou,[1]* Nina Morgner,[1]* Nelson P. Barrera,[2,3]* Argyris Politis,[1] Shoshanna C Isaacson,[1] Dijana Matak-Vinković,[2] Takeshi Murata,[4] Ricardo A. Bernal,[5] Daniela Stock,[6,7] Carol V. Robinson[1]†

The ability of electrospray to propel large viruses into a mass spectrometer is established and is rationalized by analogy to the atmospheric transmission of the common cold. Much less clear is the fate of membrane-embedded molecular machines in the gas phase. Here we show that rotary adenosine triphosphatases (ATPases)/synthases from *Thermus thermophilus* and *Enterococcus hirae* can be maintained intact with membrane and soluble subunit interactions preserved in vacuum. Mass spectra reveal subunit stoichiometries and the identity of tightly bound lipids within the membrane rotors. Moreover, subcomplexes formed in solution and gas phases reveal the regulatory effects of nucleotide binding on both ATP hydrolysis and proton translocation. Consequently, we can link specific lipid and nucleotide binding with distinct regulatory roles.

Rotary ATPases/synthases are membrane-associated molecular machines that perform biological energy conversion. Both V-type and F-type complexes consist of two reversible motors: the ion pump/turbine in V_O/F_O and the chemical motor/generator in V_1/F_1. The mode of operation is influenced by the ratio of the two fuels (protons:ATP) that drive the two motors. (*1*–*3*). The membrane-embedded V_O/F_O domain mediates the movement of Na^+ or protons across the membrane, whereas V_1/F_1 domains interact with nucleotides and inorganic phosphate either to produce or consume ATP in the case of the eukaryotic F- and V-type families, respectively. Eubacteria and archaea typically have only one type of rotary ATPase/synthase for both functions. Most bacteria have complexes of the F-type, but some bacteria and all known archaea have complexes closely related to eukaryotic V-type ATPases [also known as A-type ATPases/synthases (*4*)]. Whether of F- or V-type, the physiological function of most prokaryotic complexes is ATP synthesis; however, many have evolved regulatory functions that allow reversal into ATP-driven proton pumps if required.

F_1-F_O, and V_1-V_O, are mechanically coupled by a central rotating shaft and held together by peripheral stalks (Fig. 1). Structural details derive from isolated subcomplexes of F_1 and V_1 (*5*–*7*) and from membrane embedded proteolipid rings of various species (*8*–*11*). Despite this wealth of structural information, no high-resolution structures of any intact rotary ATPases/synthases have been reported. Thus, regulatory allosteric changes that involve both the soluble head and the membrane sector are lost. In addition heterogeneous interactions with lipids and nucleotides are difficult to observe with existing structural biology approaches.

We show using electrospray mass spectrometry (MS) that rotary ATPases/synthases from *Thermus thermophilus* (*Tt*ATPase) and *Enterococcus hirae* (*Eh*ATPase) can remain intact in the gas phase. Previously, composite models were assembled of the intact *Tt*ATPase by low-resolution electron microscopy (EM) data in combination with high-resolution x-ray structures of subunits (*12*), whereas the first cryo-EM data revealed views of the entire membrane-embedded region (*13*). We compared the MS of the two complexes, the *Tt*ATPase with that of the less well characterized *Eh*ATPase. Current models suggest that the *Eh*ATPase has only one peripheral stalk (*14*), and the stoichiometry of the K subunits in the membrane ring was determined as seven from EM (*15*) and 10 from x-ray analysis (*8*).

*Tt*ATPase was purified as described (*16*) with dodecyl maltoside (DDM) for solubilization, because under these conditions the complex is most stable and does not form aggregates. The complex was introduced into a mass spectrometer modified for high-mass complexes (*17*). Well-resolved charge states were assigned to the intact particle consisting of 26 subunits and nine different proteins (Fig. 1A). An experimentally determined mass of 659,202 (±131) dalton corresponds to that calculated for the intact complex, on the basis of subunit masses determined by MS (table S1), plus additional mass due to incomplete desolvation, and lipid and nucleotide binding (fig. S1). Gas-phase activation is necessary to release the complex from its detergent micelle (*18*, *19*), giving rise to peaks at higher mass/charge ratio (*m/z*) than the intact

[1]Department of Chemistry, Physical and Theoretical Chemistry Laboratory, University of Oxford, Oxford OX1 3QZ, UK. [2]Department of Chemistry, Lensfield Road, University of Cambridge, Cambridge CB2 1EW, UK. [3]Department of Physiology, Pontificia Universidad Católica de Chile, Alameda 340, Santiago, Chile. [4]Department of Chemistry, Graduate School of Science, Chiba University, 1-33 Yayoi-cho, Inage, Chiba 263-8522, Japan. [5]Department of Chemistry, University of Texas at El Paso, El Paso, TX 79968, USA. [6]The Victor Chang Cardiac Research Institute, Lowy Packer Building, 405 Liverpool Street, Darlinghurst NSW 2010, Australia. [7]Faculty of Medicine, University of New South Wales, Sydney 2052, Australia.

*These authors contributed equally to this work.
†To whom correspondence should be addressed. E-mail: carol.robinson@chem.ox.ac.uk

complex, formed by unfolding and dissociation of highly charged subunits, predominantly subunits E, G, and I (*20*) (fig. S2). At lower m/z, charge states are assigned to the membranous subcomplex V_O (ICL_{12}), their bimodal distribution implying that they are formed both in solution and gas phases. The corresponding soluble V_1 complex is also observed, confirming that under these solution conditions a proportion of the complex dissociates spontaneously (*21*) (fig. S3).

Using similar experimental parameters, we recorded a spectrum for the *Eh*ATPase isolated in DDM, where its functional activity has been established previously (*22*, *23*). The membrane-embedded rotor for this complex is larger because each K subunit contains four transmembrane helices as compared with two for the corresponding L subunits from *Tt*ATPase. Under conditions in which the complex emerges from the micelle surviving intact, the spectrum is not well resolved (fig. S4). Increases in activation energy lead to better desolvation and also appearance of subcomplexes in which either the membrane ring remains but the peripheral stalks and subunit I have dissociated, or the stalk subunits are attached but the membrane region is disrupted (Fig. 1B and fig. S5). The number of peripheral stalks was determined as two and the stoichiometry in the K ring as 10 (175 kD) (fig. S6).

The lipid components in the K_{10} ring were identified as a series of negatively charged cardiolipins (figs. S2 and S7 and table S2). The stoichiometry of lipid binding was determined as 10 from the mass of the membrane ring. We identified six cardiolipin isomers and, from quantitative analysis and measurement of the protein concentration, deduce specific binding of one lipid per subunit [*Eh* K subunit 1: 1.2 ± 0.1 cardiolipins (fig. S8)]. Previously, the lipids were located based on the atomic structure of the isolated K_{10} ring, in which peaks of positive density were attributed to 20 bifurcated phosphatidylglycerol lipids (*8*). We docked 10 negatively charged symmetric cardiolipins inside the K_{10} ring, proximal to the conserved Lys^{32}. The four hydrophobic chains are positioned with two chains emanating from both sides of the polar head, thus providing a hydrophobic lining to the inside of the ring (Fig. 2A).

For the *Tt*ATPase L_{12} ring, we identified the bound lipid as phosphatidylethanolamine (PE) (Fig. 2 and fig. S9). Unexpectedly, dissociated L subunits were observed either with bound PE lipid (*holo*) or without lipid (*apo*) after tandem MS of a subcomplex containing the membrane subunits and peripheral stalks (Fig. 2). Before disruption, the mass of the subcomplex is consistent with binding of six lipids. This means that *apo* and *holo* subunits coexist within the same complex. We confirmed this observation by quantifying the protein:lipid ratio as one L subunit: 0.55 ± 0.1 PE (i.e., one PE lipid per L subunit dimer) (fig. S10). Six equivalent binding sites for lipids in protein dimers in a 12-membered ring imply a sixfold symmetrical state. Previously, EM studies of the same preparation of the *Tt*ATPase revealed a sixfold symmetric membrane-embedded ring (Fig. 2 and fig. S11) (*16*). Both sets of data are consistent with close packing of two neighboring subunits, forming six dimers each with four transmembrane helices (TMHs), thus emulating the arrangement of C subunits in eukaryotic V-ATPases in which gene duplication has led to four TMHs per subunit (*24*, *25*). From modeling, we find that a rotation of the dimers by about 60° relative to their original orientation in the ring effectively locks six Glu^{63} residues in an occluded position, preserving lipid binding at the dimer interface. Proton transfer can occur at the remaining six active glutamates [Fig. 2, (i) to (iii)]; consequently, the proton:ATP ratio for the rotary enzyme is effectively halved.

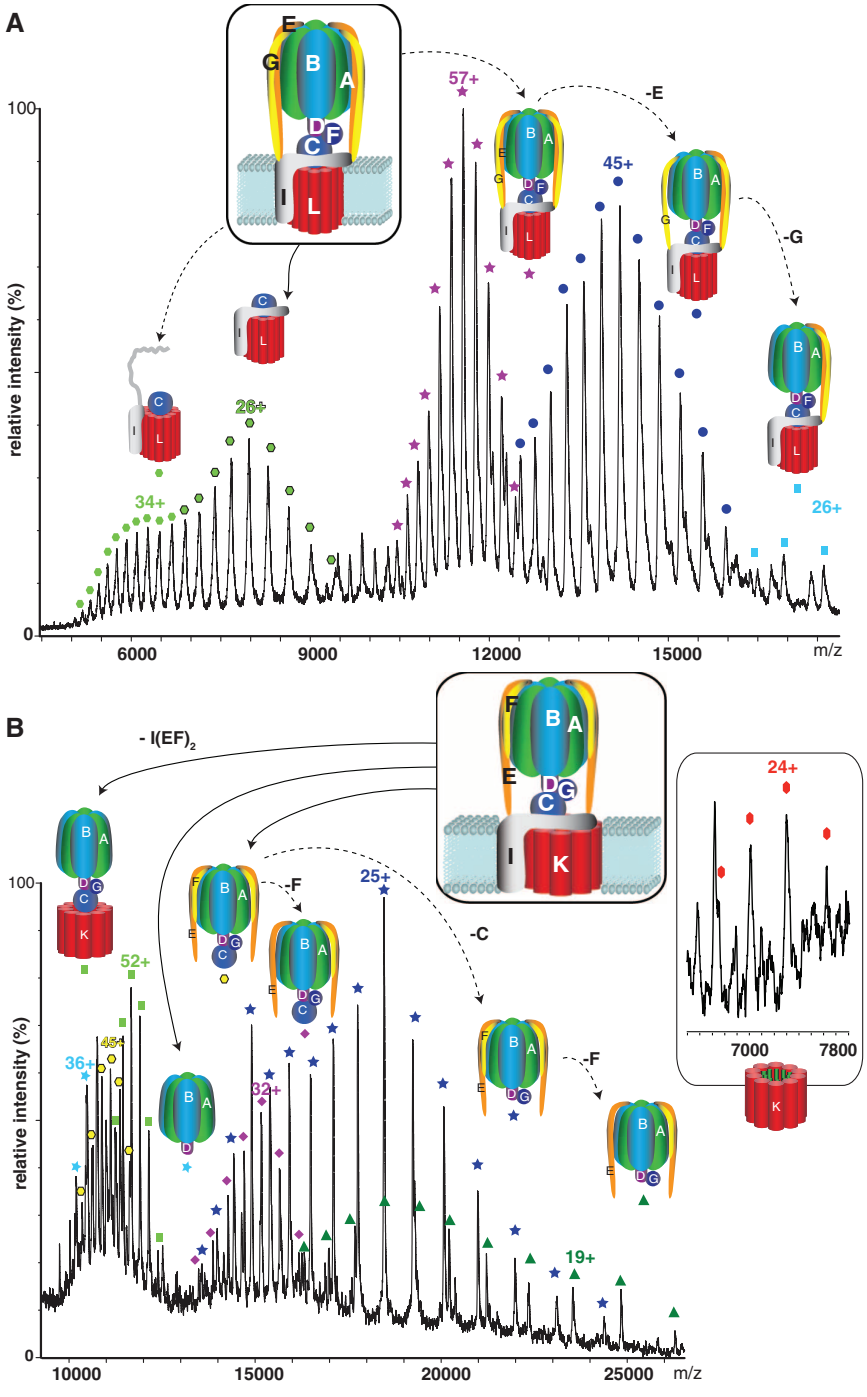

Fig. 1. Mass spectra of the intact rotary ATPases from *T. thermophilus* and *E. hirae*. (**A**) Peaks are assigned to the intact *Tt*ATPase complex (stars), loss of the membrane subcomplex (ICL_{12}) in solution and gas phases (dark green and green hexagons, respectively), and dissociation of subunits E and G from the peripheral stalk (blue circles and squares respectively). (**B**) For *Eh*ATPase, the membrane subcomplex is observed in contact with the soluble head (green squares). (Inset) Mass spectra of the K ring in aqueous solution.

In contrast to *E. hirae*, which has both F- and V-type ATPases, *T. thermophilus* has only one type of rotary ATPase that operates in both proton pumping and ATP synthesis modes in vitro (*26*). Given that each of the 12 L subunits in the *Tt*ATPase membrane ring contains only two TMHs, alternating between synthesis and pumping would involve switching the 12-membered ring from a high proton:ATP ratio, primed for synthesis (*27*), into a lower one biased for pumping (*16*). This latter scenario thus mimics the eukaryotic V-type enzyme where gene duplication has provided four TMHs each with one active glutamate. Consequently, this mechanism for switching between ATP synthesis and ion-pumping modes is likely assisted by specific lipid binding for this dual-function rotary ATPase.

These different lipid-binding patterns in the two rotary ATPases studied here were found to be invariant between repeat preparations and different detergent concentrations. Together, they provide an explanation as to how the disparate membrane rings L_{12} and K_{10} (93.6 and 160 kD) can interact with their respective C subunits (35.8 and 38.2 kD), which are likely conserved. Lining with cardiolipin, bound specifically to the inside of the K_{10} ring, reduces the orifice from 54 to 38 Å (Fig. 2A and fig. S12). Similarly, converting a 12- to a 6-membered ring for *Tt*ATPase reduces the orifice from 47 to 39 Å, creating two very similar inner diameters (38 and 39 Å) (Fig. 2B).

To assess the role of nucleotides in changing subunit interactions, we compared spectra for the *Tt*ATPase, with and without addition of 50 μM ATP. In the presence of ATP, the intact complex and membrane-embedded subcomplex ICL_{12} are the predominant species formed in solution (Fig. 3A and fig. S13). When ATP is depleted, loss of subunit B leads to extensive dissociation of the soluble head. In addition, tandem MS of V_1 in the presence of ATP leads predominantly to loss of subunit F, with subsequent loss of subunit

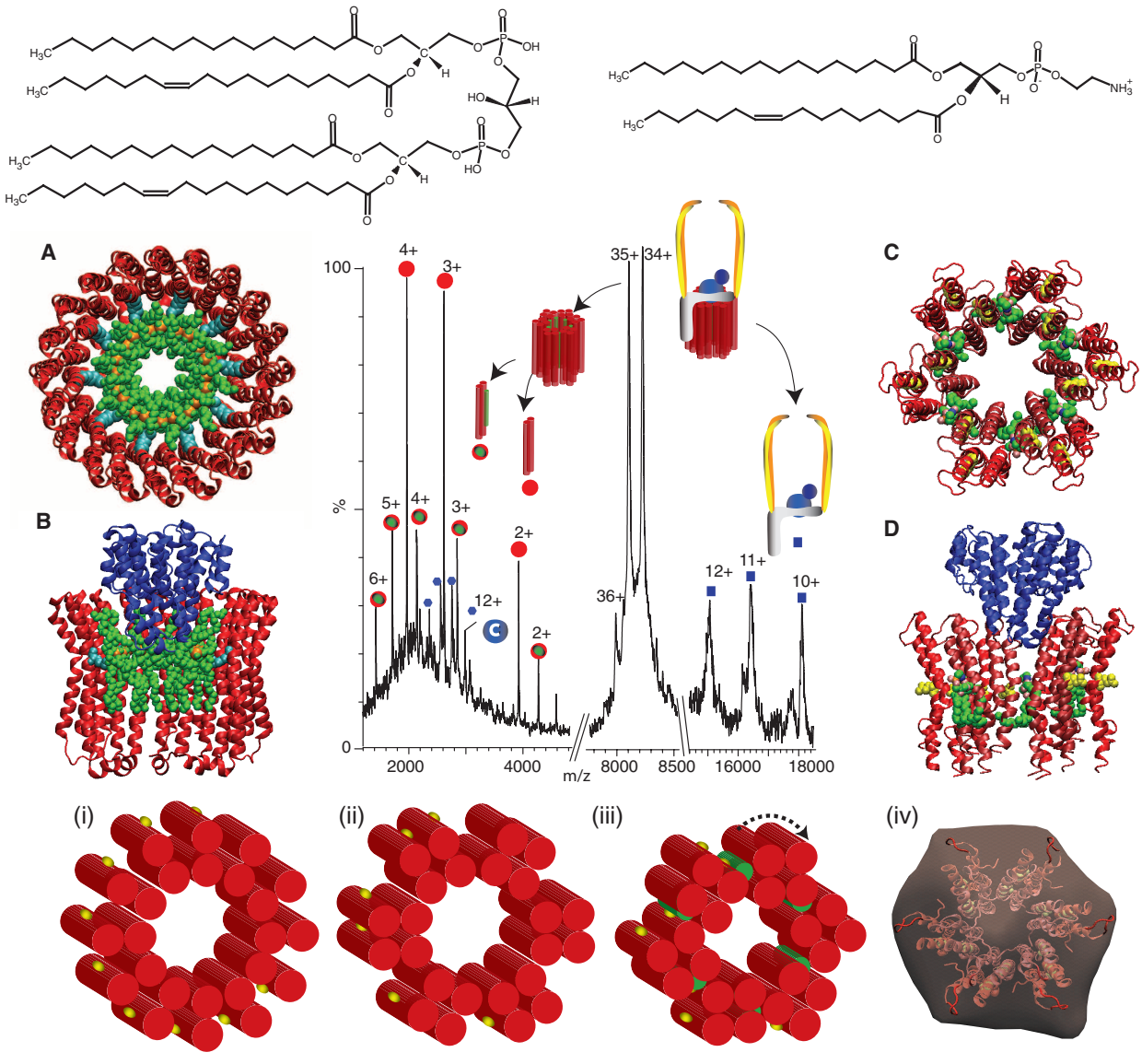

Fig. 2. Lipid binding and its effect on the membrane rings. (Upper panel) Predominant lipid molecules, one of the six cardioplipins (left) and phosphatidylethanolamine (PE, right), found in intact *Eh*ATPase and *Tt*ATPase, respectively. (Central panel) Tandem MS of a subcomplex from *Tt*ATPase [$ICL_{12}E_2G_2F$ (282 740 daltons)] leads to disruption of the L_{12} ring, releasing proteolipids L ± PE (red/green circle, 8539 daltons; red circles, 7849 daltons) and a stripped-complex ICE_2G_2F (blue squares, 184 242 daltons). Atomic structure of the K_{10} ring (*8*) of *Eh*ATPase with docking of 10 cardioplipins to show reduction in the inner diameter (**A**) and after docking subunit C (**B**). Models for sixfold symmetry of the L_{12} ring with six PE molecules (green) (**C**) and with subunit C (*42*) (blue) docked into the ring (**D**). (Lower panel) schematics of the rotor ring with 12 L subunits each having two TMHs (red cylinders) and one conserved Glu^{63} (yellow) as seen in EM of two-dimensional crystals of isolated L ring (*27*) (i). Transformation into a sixfold symmetric ring [(ii) and (iii)]. (iv) Comparison of the sixfold symmetrical model with EM data reported previously for the intact *Tt*ATPase (iv) (*16*).

D (Fig. 3B). When ATP is depleted, however, loss of subunit D before subunit F becomes possible, leaving a subcomplex with F interacting directly with the A_3B_3 hexamer. Extension of F toward the soluble head has been proposed previously as a "braking" mechanism to prevent unregulated consumption of ATP after in vivo dissociation of the head from the base in yeast V-ATPase (*28*). In line with this proposal, an x-ray structure and cryo-EM reconstruction of the isolated A_3B_3DF complex from *Tt*ATPase and yeast V-ATPase respectively, also reveal interactions of subunit F with the A_3B_3 hexamer (*7*, *29*). An x-ray structure of the auto-inhibited F_1 head of the *Escherichia coli* F-ATPase showed interactions between the subunits analogous to F_1 ε and β in the soluble head (*30*). Subjecting the *E. coli* F_1 complex to the same tandem MS procedure outlined above showed that subunit ε makes direct interactions with the soluble head (fig. S14). The similar MS dissociation patterns observed in *E. coli* F-ATPase, in which the braking mechanism is well established, and in *Tt*ATPase suggest an analogous mechanism to prevent ATP hydrolysis in the uncoupled V_1 complex of *Tt*ATPase.

We observed further sensitivity of *Tt*ATPase to low ATP concentrations, notably loss of subunit I from ICL_{12} to form CL_{12} (Fig. 3A). Expansion of the peaks assigned to ICL_{12} is consistent with binding of up to six lipids and up to two nucleotides (ATP or ADP) (fig. S15). This agrees with proposals that a eukaryotic functional equivalent of subunit I senses cellular nucleotide levels by binding selectively to ADP and undergoing conformational change (*31*). To investigate this conformational change, we applied ion mobility MS (IM-MS) (*32*) to the intact *Tt*ATPase, ICL_{12}, and CL_{12} subcomplexes. Because ions with multiple conformations result in broad arrival-time distributions (ATDs), we conclude that the relatively compact ATDs for both the intact ATPase and CL_{12} are consistent with one predominant conformation (fig. S16 and tables S3 and S4). By contrast, the ATDs for the ICL_{12} complex are much broader than those of the intact *Tt*ATPase and CL_{12}, consistent with multiple conformations of subunit I in the isolated V_O complex (Fig. 4 and table S4). The lack of conformational heterogeneity in the intact complex is rationalized by the "tethering" of subunit I by forces exerted by the peripheral stalks (subunits E and G), as suggested recently (*13*). Once released from the intact complex, subunit I in V_O is not constrained, and flexibility of the hinge domain, located between the soluble and transmembrane domains, likely leads to its conformational heterogeneity.

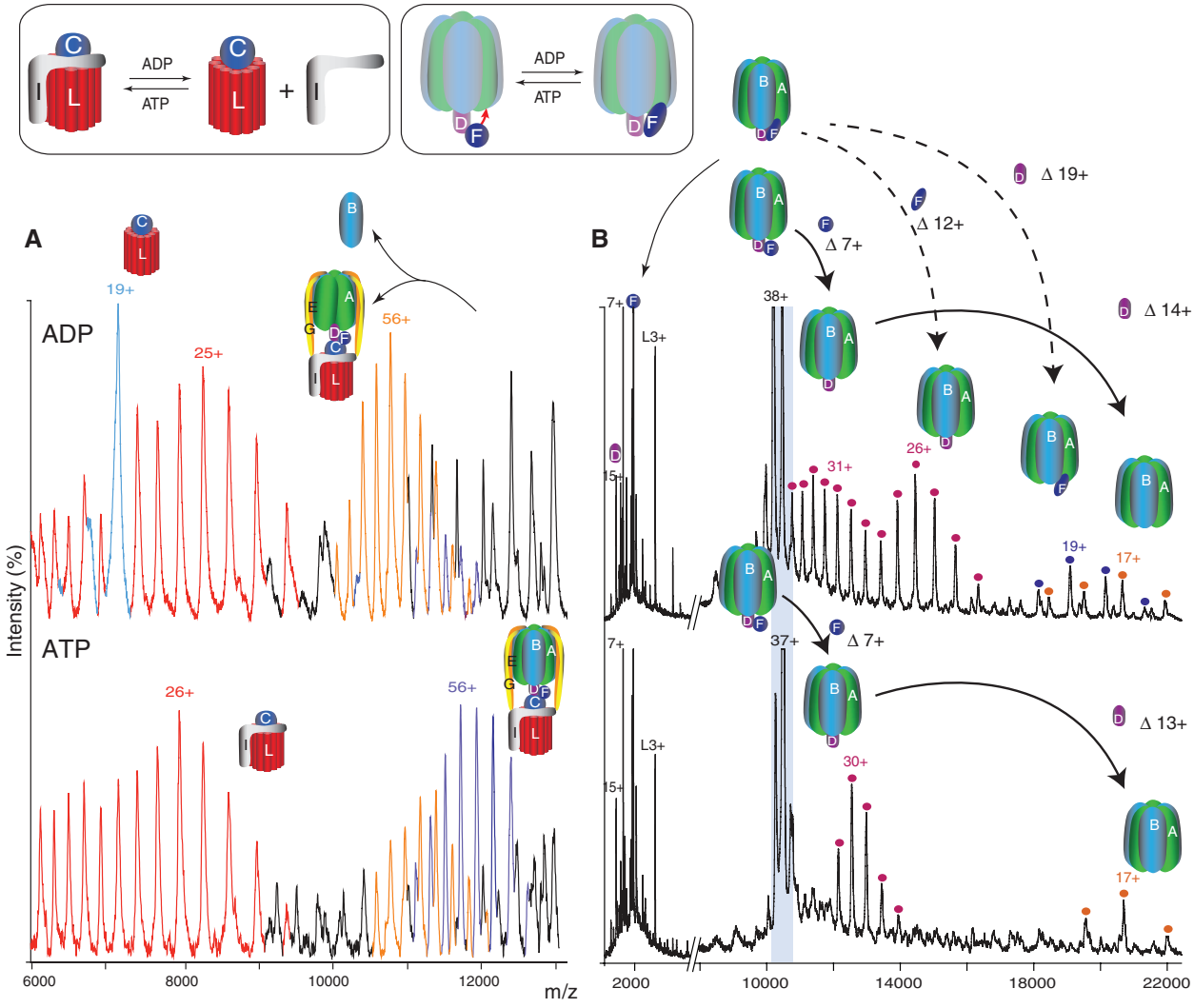

Fig. 3. Nucleotide binding and its effects on intact *Tt*ATPase and the membrane-embedded and soluble head complexes. (**A**) Depletion of ATP leads to dissociation of the B subunit from the head and subunit I from ICL_{12}. (**B**) Tandem MS of the soluble head (A_3B_3DF) reveals sequential loss of subunits F and D in the presence of 50 μM ATP. In *Tt*ATPase solutions containing 50 μM ADP, two conformations of subunit F are evident from the bimodal distribution of charge states formed for the V_1 stripped of F (Δ7+ and Δ12+) together with a direct loss of subunit D. The Δ7+ series is similar to that formed from the ATP-bound complex. The Δ12+ series is consistent with an extended conformation of subunit F. (Inset) Schematic representation of effects of ATP/ADP on the membrane ICL_{12} complex and the movement of an extended subunit F in the A_3B_3DF complex.

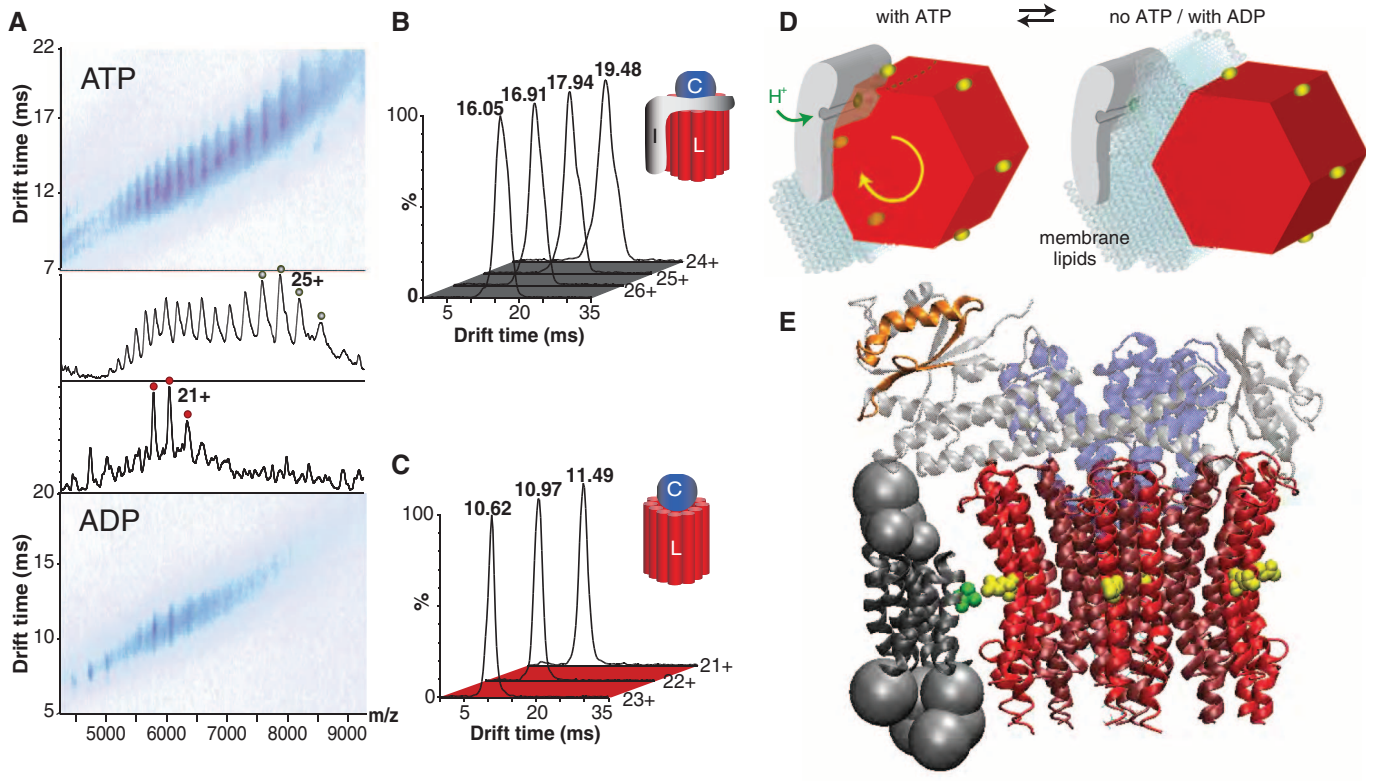

Fig. 4. Conformational heterogeneity and dissociation of subunit I from ICL_{12} implies a mechanism for closing the H^+ channel. (**A**) IM-MS of the transmembrane ICL_{12} and CL_{12} complexes formed in solution from intact *Tt*ATPase. Charge states used for IM measurement are labeled gray and red (**B** and **C**). Broader arrival-time distributions for ICL_{12} than for CL_{12} are consistent with conformational heterogenity in subunit I. (**D**) Possible mechanism to "close" the H^+ channel after lateral movement of subunit I within the membrane. Surrounding lipids effectively block the channel. The direction of proton pumping (green) and rotation of the ring (yellow) for ATP hydrolysis, as seen from the top (site of interaction with V_1). (**E**) Coarse-grained and atomic model of the ICL_{12} complex generated according to IM restraints and homology modeling (see supplementary methods). The proposed nucleotide binding area in the hinge region of I (orange) and Glu^{63}:Arg^{563} from subunits L and I are shown in yellow and green, respectively.

The soluble domain of I in EM density maps of the intact *Tt*ATPase is at 90° to the proton channel (*12*, *13*). Our IM data for the V_O complex, based on modeling of the ICL_{12} and CL_{12} complexes (fig. S17), are consistent with a range of conformational states with angles from 90° to 135° (fig. S18). We propose, therefore, that the conformational dynamics demonstrated here, together with preferential binding of ADP to the proposed site near the hinge region (*31*), destabilize interactions between I and CL_{12} as evidenced by the facile loss of subunit I under low-ATP conditions.

Given that cellular nucleotide levels likely affect proton translocation in the isolated V_O complex, it might also be anticipated that changes in the proton gradient would induce similar regulatory effects. To test this hypothesis, we increased the pH of the ATPase-containing solution to mimic reduction of the proton concentration. Mass spectra of the *Tt*ATPase incubated at pH 9.0 led to subcomplexes formed by loss of IGE (fig. S19). This observation, together with the dissociation of subunit I from V_O, suggests a regulatory role for subunit I, sensing both proton and ATP concentrations. Previous proposals invoked a locking together of the membrane portion of subunit I with the CL_{12} membrane ring, preventing relative movement and hence explaining the absence of passive H^+ translocation in isolated V_O (*33*, *34*). Because we observe facile loss of subunit I under both low–H^+ concentration ($[H^+]$) and low-[ATP] conditions, and given the lack of extensive interactions between I and the membrane ring observed in cryo-EM data (*13*), our results point to a mechanism in which subunit I moves away from the ring, and the resulting gap could then be sealed with membrane lipids (Fig. 4D).

Our results show that lipids with two and four hydrophobic chains associate with subunits with two and four TMHs—subunits L and K, respectively. In both ATPases, the lipids identified in situ are not the most prevalent ones in the cell (*35*, *36*), implying that lipids are selected from the available pool for specific structural roles and metabolic regulation. This further supports the proposal that membrane proteins possess specific lipid binding sites (*37*) and demonstrates the ability of lipids to fine tune subunit interactions by defining the conformations and inner dimensions of the membrane rings. Our nucleotide-binding experiments show that a decrease in cellular ATP concentrations is sensed by V_1, not only with the movement of subunit F but also with changes in interactions at the A:B interface. Unexpectedly, V_O is also sensitive to low [ATP] and $[H^+]$, both of which promote displacement of subunit I. We suggest that membrane lipids subsequently seal the proton-conducting channel. Consequently, both ATP and proton/ion gradients are conserved when reversible dissociation takes place in vivo.

The existence of intact rotary ATPases/synthases in vacuum has been demonstrated previously with LILBID MS (*38*, *39*). At its current resolution, however, it is not possible to identify bound lipids or nucleotides or to probe their effects on subunit interactions. Moreover, previous ES-MS experiments produced well-resolved mass spectra for the V_1 domain (*40*, *41*), but lack of an intact V_O domain, or any interactions between V_1 and V_O, is attributed to dissociation of the complex in the absence of the protective micelle (*18*, *19*). By contrast, the ES approach used here enables interrogation of subunit interactions within intact rotary ATPase/synthases and allows us to probe the synergistic effects of lipid and nucleotide binding.

References and Notes

1. K. C. Jefferies, D. J. Cipriano, M. Forgac, *Arch. Biochem. Biophys.* **476**, 33 (2008).
2. C. von Ballmoos, A. Wiedenmann, P. Dimroth, *Annu. Rev. Biochem.* **78**, 649 (2009).

3. S. P. Muench, J. Trinick, M. A. Harrison, *Quat. Rev. Biophys.* **44**, 311 (2011).
4. V. Müller, G. Grüber, *Cell. Mol. Life Sci.* **60**, 474 (2003).
5. J. P. Abrahams, A. G. Leslie, R. Lutter, J. E. Walker, *Nature* **370**, 621 (1994).
6. K. Okazaki, S. Takada, *Structure* **19**, 588 (2011).
7. N. Numoto, Y. Hasegawa, K. Takeda, K. Miki, *EMBO Rep.* **25**, 25 (2009).
8. T. Murata, I. Yamato, Y. Kakinuma, A. G. Leslie, J. E. Walker, *Science* **308**, 654 (2005).
9. T. Meier, P. Polzer, K. Diederichs, W. Welte, P. Dimroth, *Science* **308**, 659 (2005).
10. A. Dautant, J. Velours, M. F. Giraud, *J. Biol. Chem.* **285**, 29502 (2010).
11. I. N. Watt, M. G. Montgomery, M. J. Runswick, A. G. Leslie, J. E. Walker, *Proc. Natl. Acad. Sci. U.S.A.* **107**, 16823 (2010).
12. L. K. Lee, A. G. Stewart, M. Donohoe, R. A. Bernal, D. Stock, *Nat. Struct. Mol. Biol.* **17**, 373 (2010).
13. W. C. Lau, J. L. Rubinstein, *Proc. Natl. Acad. Sci. U.S.A.* **107**, 1367 (2010).
14. M. Yamamoto *et al.*, *J. Biol. Chem.* **283**, 19422 (2008).
15. T. Murata *et al.*, *J. Biol. Chem.* **278**, 21162 (2003).
16. R. A. Bernal, D. Stock, *Structure* **12**, 1789 (2004).
17. H. Hernández, C. V. Robinson, *Nat. Protoc.* **2**, 715 (2007).
18. N. P. Barrera, N. Di Bartolo, P. J. Booth, C. V. Robinson, *Science* **321**, 243 (2008).
19. N. P. Barrera *et al.*, *Nat. Methods* **6**, 585 (2009).
20. J. L. Benesch, C. V. Robinson, *Curr. Opin. Struct. Biol.* **16**, 245 (2006).
21. K. Yokoyama *et al.*, *J. Biol. Chem.* **278**, 42686 (2003).
22. K. Takase *et al.*, *J. Biol. Chem.* **269**, 11037 (1994).
23. T. Murata, K. Takase, I. Yamato, K. Igarashi, Y. Kakinuma, *J. Biochem.* **125**, 414 (1999).
24. M. Mandel *et al.*, *Proc. Natl. Acad. Sci. U.S.A.* **85**, 5521 (1988).
25. D. K. Clare *et al.*, *Structure* **14**, 1149 (2006).
26. K. Yokoyama *et al.*, *J. Biol. Chem.* **275**, 13955 (2000).
27. M. Toei *et al.*, *Proc. Natl. Acad. Sci. U.S.A.* **104**, 20256 (2007).
28. P. M. Kane, A. M. Smardon, *J. Bioenerg. Biomembr.* **35**, 313 (2003).
29. Z. L. Hildenbrand, S. K. Molugu, D. Stock, R. A. Bernal, *PLoS ONE* **5**, e12588 (2010).
30. G. Cingolani, T. M. Duncan, *Nat. Struct. Mol. Biol.* **18**, 701 (2011).
31. A. Armbrüster *et al.*, *FEBS Lett.* **579**, 1961 (2005).
32. C. Uetrecht, R. J. Rose, E. van Duijn, K. Lorenzen, A. J. Heck, *Chem. Soc. Rev.* **39**, 1633 (2010).
33. J. Zhang, M. Myers, M. Forgac, *J. Biol. Chem.* **267**, 9773 (1992).
34. C. Beltrán, N. Nelson, *Acta Physiol. Scand. Suppl.* **607**, 41 (1992).
35. D. Carson, R. A. Pieringer, L. Daneo-Moore, *Biochim. Biophys. Acta* **575**, 225 (1979).
36. P. H. Ray, D. C. White, T. D. Brock, *J. Bacteriol.* **108**, 227 (1971).
37. C. Hunte, S. Richers, *Curr. Opin. Struct. Biol.* **18**, 406 (2008).
38. T. Meier *et al.*, *Mol. Microbiol.* **65**, 1181 (2007).
39. J. Hoffmann *et al.*, *Phys. Chem. Chem. Phys.* **12**, 13375 (2010).
40. O. Esteban *et al.*, *J. Biol. Chem.* **283**, 2595 (2008).
41. N. Kitagawa, H. Mazon, A. J. Heck, S. Wilkens, *J. Biol. Chem.* **283**, 3329 (2008).
42. M. Iwata *et al.*, *Proc. Natl. Acad. Sci. U.S.A.* **101**, 59 (2004).

Acknowledgments: Funding from the Wellcome Trust and by the PROSPECTS (HEALTHF4-2008-201648) grant within the Research Framework of the European Union together with funding from the Royal Society (C.V.R.), the Australian National Health and Medical Research Council grant 573712 (D.S.), and the FONDECYT 1100515 (N.P.B.) is acknowledged.

Supporting Online Material

www.sciencemag.org/cgi/content/full/334/6054/380/DC1
Materials and Methods
Figs. S1 to S19
Tables S1 to S4
References (*43*–*58*)

22 June 2011; accepted 15 September 2011
10.1126/science.1210148

Cerebellum Shapes Hippocampal Spatial Code

Christelle Rochefort,[1]* Arnaud Arabo,[1]*† Marion André,[2]‡ Bruno Poucet,[2] Etienne Save,[2]* Laure Rondi-Reig[1]*§

Spatial representation is an active process that requires complex multimodal integration from a large interacting network of cortical and subcortical structures. We sought to determine the role of cerebellar protein kinase C (PKC)–dependent plasticity in spatial navigation by recording the activity of hippocampal place cells in transgenic L7PKCI mice with selective disruption of PKC-dependent plasticity at parallel fiber–Purkinje cell synapses. Place cell properties were exclusively impaired when L7PKCI mice had to rely on self-motion cues. The behavioral consequence of such a deficit is evidenced here by selectively impaired navigation capabilities during a path integration task. Together, these results suggest that cerebellar PKC-dependent mechanisms are involved in processing self-motion signals essential to the shaping of hippocampal spatial representation.

It is well established that rodents build an internal cognitive map to navigate in their environment. A key neural substrate enabling such representation is the hippocampus, which contains CA1 and CA3 pyramidal cells described as place cells. Each place cell fires for a restricted region (the place field) of the environment (*1*, *2*). Both external cues and self-motion cues (i.e., vestibular, proprioceptive, and optic flow cues) control place cell firing (*3*, *4*), which suggests the involvement of a large network of cortical and subcortical structures interacting with the hippocampus for navigation. Determining the functional architecture of such a network is thus essential to our understanding of how the hippocampal place cell code is generated. The medial entorhinal cortex, a key relay structure between neocortical areas and the hippocampus, contains grid cells with regularly spaced multiple firing fields (*5*), which integrate self-motion information and participate in path integration (*4*, *6*, *7*).

The cerebellum has also been shown to be essential to the processing of self-motion information: Cerebellar Purkinje cells respond to vestibular signals by transforming head-centered vestibular afferent information into Earth-reference self-motion and spatial orientation signals (*8*, *9*), and electrophysiological investigations suggest that the cerebellum and the hippocampus can be functionally connected during eyeblink conditioning (*10*, *11*). However, it is still unknown whether such an interaction is functionally relevant in navigation, and a mechanism that might underlie such a process has not been identified.

In the transgenic mouse strain L7PKCI, the pseudosubstrate protein kinase C inhibitor (PKCI) is selectively expressed in Purkinje cells under the control of the *pcp-2* (L7) gene promoter (*12*). This results in an impaired long-term depression (LTD) at cerebellar parallel fiber–Purkinje cell synapses. Such a plasticity mechanism has been proposed to work as an error-based (anti-Hebbian) learning process (*13*, *14*) during conditioning tasks (*15*) and in optimization of motor response during navigation (*16*).

A total of 506 dorsal CA1 hippocampal cells were recorded. A subset of 150 place cells was further analyzed in six L7PKCI mice and five wild-type littermate control mice. Relative to wild-type mice, L7PKCI mice had a significantly lower proportion of place cells [L7PKCI, $n = 53/218$ (24.3%); wild type, $n = 97/288$ (33.7%); $\chi^2 = 5.2$, df = 1, $P < 0.025$]. Neural activity was sampled as the mice freely explored a circular arena containing a salient cue (a card with a bottle attached to it), in standard sessions (S1 and S2) and involving cue manipulation in subsequent sessions (S3 and S4). A last session (S5) similar to sessions S1 and S2 was run to determine whether we could restore the initial firing pattern irrespective of the changes in cell firing observed during the cue manipulation sessions (Fig. 1A) (*17*).

After recording in the standard sessions, we used two distinct environmental manipulations, cue removal and cue conflict, in which mice are forced to use self-motion cues. In the cue removal condition, the arena was in the dark and the cue

[1]Neurobiologie des Processus Adaptatifs (UMR 7102), Navigation, Memory, and Aging (ENMVI) Team, Université Pierre et Marie Curie–Centre National de la Recherche Scientifique (CNRS), F-75005 Paris, France. [2]Laboratory of Neurobiology and Cognition (UMR 6155), Aix Marseille Université–CNRS, 3 place Victor Hugo, 13331 Marseille, France.

*These authors contributed equally to this work.
†Present address: Laboratoire de Psychologie et Neurosciences de la Cognition et de l'Affectivité (EA 4306), Université de Rouen, Faculté des Sciences, Place Emile Blondel, 76821 Mont-Saint-Aignan Cedex, France.
‡Present address: Department of Experimental Neurophysiology, Ruhr University Bochum, Universitätsstrasse 150, MABF 01/551, 44801 Bochum, Germany.
§To whom correspondence should be addressed. E-mail: laure.rondi@snv.jussieu.fr

Mass Spectrometry of Intact V-Type ATPases Reveals Bound Lipids and the Effects of Nucleotide Binding

Min Zhou, Nina Morgner, Nelson P. Barrera, Argyris Politis, Shoshanna C Isaacson, Dijana Matak-Vinkovic, Takeshi Murata, Ricardo A. Bernal, Daniela Stock and Carol V. Robinson (October 20, 2011)

Science **334** (6054), 380-385. [doi: 10.1126/science.1210148]

Editor's Summary